

# Optimal Investment Portfolio of Thyristor- and IGBT-based Electrolysis Rectifiers in Utility-scale Renewable P2H Systems

Yangjun Zeng, *Student Member, IEEE*, Yiwei Qiu, *Member, IEEE*, Liuchao Xu, Chenjia Gu, *Member, IEEE*, Yi Zhou, *Member, IEEE*, Jiarong Li, *Member, IEEE*, Shi Chen, *Member, IEEE*, and Buxiang Zhou, *Member, IEEE*

**Abstract**—Renewable power-to-hydrogen (ReP2H) systems require rectifiers to supply power to electrolyzers (ELZs). Two main types of rectifiers, insulated-gate bipolar transistor rectifiers (IGBT-Rs) and thyristor rectifiers (TRs), offer distinct tradeoffs. IGBT-Rs provide flexible reactive power control but are costly, whereas TRs are more affordable with lower power loss but consume a large amount of uncontrollable reactive power. A mixed configuration of rectifiers in utility-scale ReP2H systems could achieve a decent tradeoff and increase overall profitability. To explore this potential, this paper proposes an optimal investment portfolio model. First, we model and compare the active and reactive power characteristics of ELZs powered by TRs and IGBT-Rs. Second, we consider the investment of ELZs, rectifiers, and var resources and coordinate the operation of renewables, energy storage, var resources, and the on-off switching and load allocation of multiple ELZs. Subsequently, a two-stage stochastic programming (SP) model based on weighted information gap decision theory (W-IGDT) is developed to address the uncertainties of the renewable power and hydrogen price, and we apply the progressive hedging (PH) algorithm to accelerate its solution. Case studies demonstrate that optimal rectifier configurations increase revenue by at most 2.56% compared with using only TRs or IGBT-Rs, as well as those in existing projects. Under the optimal portfolio, reactive power compensation investment is nearly eliminated, with a preferred TR-to-IGBT-R ratio of 3:1.

**Index Terms**—renewable power-to-hydrogen, electrolyzer, rectifier, investment portfolio, reactive power, stochastic programming

## NOMENCLATURE

### A. Abbreviations

BES	Battery energy storage
ELZ	Electrolyzer
IGBT-R	Insulated-gate bipolar transistor-based rectifier
OLTC	On-load tap changer
PV	Photovoltaic
ReP2H	Renewable power-to-hydrogen
SP	Stochastic programming
TR	Thyristor rectifier
W-IGDT	Weighted information gap decision theory
WT	Wind turbine

### B. Indices and Sets

$n, t$	Index for ELZs and time periods
--------	---------------------------------

Financial support was obtained from the National Key R&D Program of China (2021YFB4000503) and the National Natural Science Foundation of China (52377116 and 52307126). (*Corresponding author: Yiwei Qiu*)

Y. Zeng, Y. Qiu, L. Xu, C. Gu, Y. Zhou, S. Chen, and B. Zhou are with the College of Electrical Engineering, Sichuan University, Chengdu 610065, China. (ywqiu@scu.edu.cn)

J. Li is with the Harvard John A. Paulson School of Engineering and Applied Sciences, Harvard University, Cambridge 02138, USA.

$i, j, j'$	Index for buses
$ij$	Index for branches
$\pi(j), \sigma(j)$	Set of parents and children of bus $j$

### C. Variables

#### 1) Investment Variables:

$\sigma^{\text{ELZ}}$	Number of ELZs
$\sigma^{\text{TR}}, \sigma^{\text{IGBT}}$	Number of TR and IGBT-R
$W^{\text{C}}$	Capacity of var compensation

#### 2) Operational Variables:

$P^{\text{Stack}}, U^{\text{Stack}}$	DC power and voltage of the stack
$I, Y^{\text{H}_2}$	Electrolytic current and hydrogen flow
$T$	Stack temperature of the ELZ
$b^{\text{On}}, b^{\text{By}}, b^{\text{Idle}}$	Production, standby, and idle states
$b^{\text{SU}}, b^{\text{SD}}$	Startup/shutdown actions of ELZ
$P^{\text{ELZ}}, Q^{\text{ELZ}}$	Active/reactive power of the ELZ
$P^{\text{Rec}}$	Active power of the rectifier of the ELZ
$Q^{\text{TR}}, Q^{\text{IGBT}}$	Reactive power of the TR and IGBT-R
$P^{\text{BoP}}$	Power of the balance of plant of the ELZ
$P^{\text{Loss}}$	The active loss of the TR/IGBT-R of the ELZ
$P^{\text{Heat}}, P^{\text{Diss}}$	Electrolytic heat and dissipation of the ELZ
$P^{\text{Cool}}$	Cooling heat flow of the ELZ
$P_{ij,t}, Q_{ij,t}$	Active/reactive power flows on branch $ij$
$I_{ij,t}, \ell_{ij,t}$	Current on branch $ij$ and its square
$U_{j,t}, v_{j,t}$	Voltage amplitude of bus $j$ and its square
$p_{j,t}, q_{j,t}$	Active/reactive power injections at bus $j$
$p_{j,t}^{\text{L}}, q_{j,t}^{\text{L}}$	Active/reactive loads of all ELZs at bus $j$
$P_{j,t}^{\text{WT}}, Q_{j,t}^{\text{WT}}$	Active/reactive power of the WT at bus $j$
$P_{j,t}^{\text{PV}}, Q_{j,t}^{\text{PV}}$	Active/reactive power of the PV at bus $j$
$E_{j,t}$	Energy stored level of the BES at bus $j$
$P_{j,t}^{\text{BES,C/D}}$	BES charging/discharging power at bus $j$
$b_{j,t}^{\text{BES,C/D}}$	BES Charging/discharging states at bus $j$
$Q_{j,t}^{\text{BES/C}}$	Reactive power of the BES/var comp. at bus $j$
$k_{ij,t}, \delta_{ij,k,t}$	Turn ratio of the OLTC and its binary decision on the $k$ th level of the transformer $ij$

### D. Parameters

$N_s$	The product of the number of typical days and the number of hydrogen price scenarios
$N_t, \Delta t$	Scheduling horizon and step length
$c^{\text{ELZ}}$	Investment cost of ELZ
$c^{\text{TR}}, c^{\text{IGBT}}$	Investment costs of TR and IGBT-R
$c^{\text{C}}$	Investment cost of var compensation
$c^{\text{H}_2}$	Hydrogen price
$c^{\text{SU}}, c^{\text{SD}}$	Startup/shutdown costs of the ELZ
$\bar{\sigma}^{\text{ELZ}}$	Upper limit of the number of ELZs
$\bar{I}, \underline{I}$	Electrolytic current limits of the ELZ

$\bar{T}, T$	Stack temperature limits of the ELZ
$\eta^{\text{Cool}}$	Cooling efficiency of the ELZ
$P^{\text{By}}$	Standby power consumption of the ELZ
$C^{\text{ELZ}}, R^{\text{Diss}}$	Heat capacity and dissipation resistance of ELZ
$T^{\text{Am}}$	Ambient temperature
$c^{\text{Cool}}, T^{\text{Cool}}$	Cooling factor and coolant temperature of ELZ
$r_{ij}, x_{ij}$	Resistance and reactance of branch $ij$
$\bar{U}_j, \underline{U}_j$	Voltage magnitude limits at bus $j$
$\bar{I}_{ij}$	Current capacity limit of branch $ij$
$S_j^{\text{WT/PV/BES}}$	WT/PV/BES installation capacities at bus $j$
$S^{\text{sc}}$	Short-circuit capacity at hydrogen plant node
$S^{\text{TR/IGBT}}$	Rated capacities of TR/IGBT-R
$\theta$	Minimum power factor angle of PV plants
$\bar{P}^{\text{BES,C/D}}$	BES charging/discharging power limits
$\eta^{\text{BES,C/D}}$	BES charging/discharging efficiencies
$\zeta^{\text{BES}}$	BES self-discharge ratio
$\bar{E}, \underline{E}$	Energy stored level limits of the BES
$\bar{k}_{ij}^{\text{All}}$	OLTC switching time limit of transformer $ij$
$\bar{k}_{ij}, \underline{k}_{ij}$	OLTC ratio limits of transformer $ij$

## I. INTRODUCTION

### A. Background and Motivation

**R**ENEWABLE power-to-hydrogen (ReP2H) facilitates wind and solar integration [1] and has significant potential for applications in energy storage, transportation [1], and the chemical industry [2]. With the continuous growth of renewable energy installations, the ReP2H industry has grown rapidly under policy incentives and market drivers [3], [4], leading to increased investment in electrolyzers (ELZs) in large-scale hydrogen plants to replace fossil-based hydrogen production.

Industrial hydrogen plants typically consist of multiple ELZs [5], each integrating a rectifier, an electrolytic stack, and the balance of plant (BoP) [6]. Since electrolytic stacks operate on DC power, rectifiers are required to convert AC to DC. Currently, two types of rectifiers are commercially available: thyristor rectifiers (TRs) and insulated-gate bipolar transistor-based rectifiers (IGBT-Rs) [7]. They offer distinct tradeoffs, as summarized in Table I.

IGBT-Rs use PWM modulation and voltage vector control, enabling independent active and reactive power control. Thus, IGBT-Rs can maintain a power factor (PF) of 1 on the AC side [8] or provide flexible reactive power support [9], or even enable voltage ride-through [10]. Moreover, their fast response makes IGBT-Rs well suited for weak or off-grid systems [11]. However, their structural complexity leads to higher costs and power losses.

TRs are more mature and widely applied in low-voltage high-current applications such as water and chlor-alkali electrolysis. They employ multipulse (usually 12–48) rectification to reduce harmonics. They are more cost-effective and efficient than IGBT-Rs. However, owing to their phase-controlled nature, TRs consume a large amount of reactive power, and the active and reactive power components are coupled [12]. Thus, additional var resources, such as compensators and on-load tap changers (OLTCs), are often required to ensure voltage security [6], [12].

In practice, some large-scale projects [13], [14] use mixed rectifier (MR) configurations to leverage the complementary

TABLE I  
COMPARISON OF TR AND IGBT-R POWERING A 5-MW ELECTROLYZER

Rectifier	Reactive power characteristics	Investment cost (CNY)	Efficiency
TR <sup>1</sup>	Coupled with active load [12]; see Fig. 4(a)	≈1 million	≈98% [16]
IGBT-R	PF=1 [8]; or to provide and absorb reactive power decoupled from active load [9], [10]; see Fig. 4(b)	2 to 3 million	≈97% [16]

<sup>1</sup> Experiments [16], [17] have shown that a 24-pulse TR can control total harmonic distortion (THD) of current to 3–5% (the IGBT-R is even better), which can meet the power grid regulation with filters. Therefore, this study does not consider the harmonics of either type and leaves this topic to future work.

characteristics of TRs and IGBT-Rs. The *China Energy Engineering Songyuan Hydrogen Industry Park* [13] in Songyuan, China, employs 12 TRs and 24 IGBT-Rs to power 36 alkaline ELZs, and the *Wind-Solar Hydrogen-Ammonia Integration Project* [14] in Da'an, China, uses 32 TRs and 32 IGBT-Rs for 64 ELZs. However, to the best of the author's knowledge, such configurations have not been quantitatively analyzed. Suboptimal configurations may lead to excessive or insufficient reactive power compensation, increasing investment or operating costs.

Moreover, our previous research [6], [15] revealed that TR-powered ELZs face tradeoffs between efficiency and the reactive load. This means that the investment and operation of the ReP2H system should be coordinated in terms of both active and reactive power. However, existing ReP2H planning research has focused mainly on the sizing of energy sources and ELZs while considering only active power and neglecting rectifier selection and var resources. An optimal investment decision from the perspective of active and reactive power coordination is vital for improving capital efficiency, which, unfortunately, has not been investigated.

### B. Literature Review and Research Gap

ReP2H planning research typically addresses renewable energy, battery energy storage (BES), ELZs, and hydrogen storage (HS). For example, Li *et al.* [18] proposed an investment model for ELZs and seasonal HS, considering power and hydrogen delivery, to address the spatiotemporal imbalance between renewable resources and hydrogen demand. Pan *et al.* [19] developed a robust capacity sizing model for wind turbines (WTs), photovoltaics (PVs), ELZs, and HSs in integrated energy systems. Zhu *et al.* [20] proposed an energy management framework and studied BES capacity sizing in off-grid ReP2H systems. Li *et al.* [21] explored the configuration of the number and size of ELZs and developed operation rules to enhance wind power integration. To assess the cost competitiveness of green hydrogen, Ibáñez-Rioja *et al.* [22] optimized planning and operation using 30 years of real-world wind and solar data. Similarly, Zheng *et al.* [23] analyzed the levelized cost of hydrogen (LCOH) for off-grid wind P2H systems and reported that optimal sizing reduces LCOH.

However, the aforementioned studies [18]–[23] overlooked rectifier configuration and reactive power balance in ReP2H planning. Given that rectifiers account for 20–30% of ELZ investment [24], their optimal selection is crucial for economic feasibility. Current research on rectifiers for hydrogen production has focused mainly on performance analysis [8], [12] or short-term scheduling [6], [15].

For example, Ruuskanen *et al.* [12] investigated the power quality and reactive power characteristics of ELZs powered by

TRs. Koponen *et al.* [8] compared the tradeoffs of the TR and IGBT-R in terms of performance and investment in industrial applications. In our prior work [6], [15], Li *et al.* [15] integrated rectifier power characteristics into ReP2H scheduling, revealing conflicts between productivity and the grid-side PF in grid-connected hydrogen plants, whereas Zeng *et al.* [6] addressed the tradeoffs between P2H energy conversion efficiency and network losses caused by the reactive power of a TR and proposed a coordinated power management approach for large hydrogen plants that integrate multiple ELZs.

Despite these advancements, the optimal rectifier configuration in ReP2H planning remains unaddressed. Current designs are often based on intuition [13], [14] rather than quantitative analysis. The challenge of leveraging the complementarities between TRs and IGBT-Rs to achieve an optimal tradeoff remains unexplored.

### C. Contributions of This Work

To fill the aforementioned gap and explore MR configurations for improving capital efficiency in ReP2H systems, we propose an optimal portfolio model based on stochastic programming (SP). The key contributions are as follows:

- 1) The active and reactive characteristics of TR- and IGBT-R-powered ELZs are modeled and compared, revealing their complementarity and the potential of a mixed rectifier configuration, which is incorporated into planning.
- 2) An optimal investment portfolio model for MR and var resources in ReP2H systems is proposed. The model handles uncertainties via weighted information gap decision theory (W-IGDT). A two-stage decomposition algorithm, progressive hedging (PH) [25], is applied to improve computational efficiency.
- 3) Case studies on realistic systems show that optimizing MR configuration can increase revenue by at most 2.56% compared with that of uniform configurations or those in existing projects. The results suggest that a 3:1 ratio of TRs to IGBT-Rs offers better benefits.

The rest of this paper is organized as follows. Section II presents the load characteristics of ELZs powered by TRs and IGBT-Rs. Section III establishes the investment portfolio model and corresponding solution approach. In Section IV, simulations verify the proposed model. Finally, the conclusions drawn from this work are summarized in Section V.

## II. SYSTEM STRUCTURE AND COMPARISON BETWEEN ELZS POWERED BY TR AND IGBT-R

### A. General Configuration of ReP2H Systems

On the basis of existing projects [13], [14], the general structure of an ReP2H system is illustrated in Fig. 1. The system integrates renewable energy sources (wind and solar), transmission lines, a hydrogen plant, and sometimes a BES. The hydrogen plant often comprises multiple ELZs. Owing to policy restrictions [26], power exchange with the external grid is limited and thus is not considered in this work.

The ELZs, as DC loads, may be powered by TRs or IGBT-Rs. They exhibit distinctive active and reactive load characteristics, as detailed in Section II-C. This paper assumes that TRs are commonly used 24-pulse rectifiers [16].

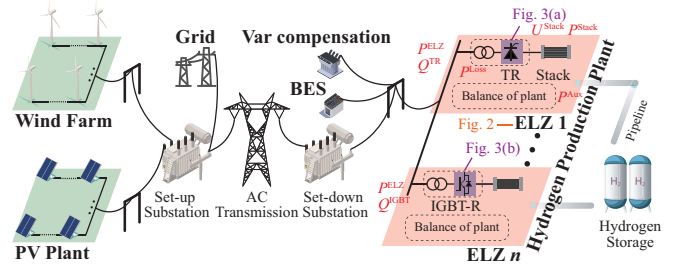


Fig. 1. The general structure of ReP2H systems.

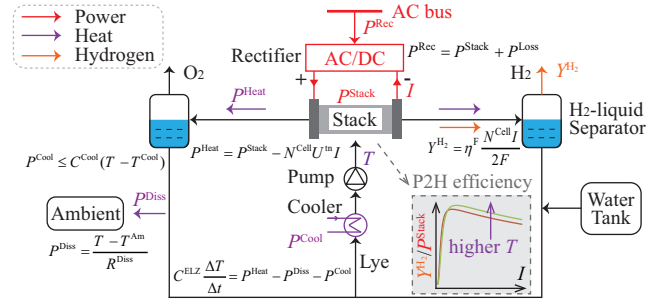


Fig. 2. Schematic diagram of an alkaline electrolyzer.

### B. Hydrogen Production, Heat, and State-switching Characteristics of Electrolyzers

A schematic diagram of an alkaline ELZ is shown in Fig. 2. TR- and IGBT-R-powered ELZs share common characteristics, including hydrogen production, temperature dynamics, and state transitions. We summarize their physical models and operational constraints in Table II.

1) *Hydrogen production and heat submodels*: The active power of an ELZ consists of stack power, BoP consumption, and rectifier losses, modeled as (1)–(4). The electrolytic voltage-current relationship follows a nonlinear U-I curve [27], given by (5), with safety and operational limits of (6).

The power consumed by the electrolytic stack partially converts into hydrogen, while the remainder dissipates as heat. The hydrogen production flow  $Y^{H_2}$  follows (7), where the Faradaic efficiency  $\eta^F$  is modeled by (8). The P2H energy conversion efficiency  $Y^{H_2}/P^{Stack}$  is significantly affected by the temperature, as shown in Fig. 2.

The temperature control relies on the coordination between the stack and BoP. Proper thermal management of the ELZ can improve P2H efficiency and reduce auxiliary power use. We use a first-order model (9) to describe the temperature dynamics [27], summarized as (10)–(13).

2) *State switching submodel*: ELZs switch among *production*, *standby*, and *idle* states to achieve a wide and flexible load range to accommodate the volatile renewable power, similar to power system unit commitment (UC). Their transitions are governed by (14)–(17) [28]. For detailed ELZ models, interested readers can refer to our prior work [5], [6].

### C. Reactive Power Characteristics

We now compare ELZs powered by TRs and IGBT-Rs in terms of reactive power and efficiency. Fig. 3 shows the topologies of a 24-pulse TR and an IGBT-R.

1) *TR*: The TR consumes a significant amount of reactive power, which is coupled with the active power and exhibits a nonlinear relationship. The relation between the reactive power

TABLE II  
PRODUCTION, HEAT, AND STATE TRANSITION MODEL OF ELECTROLYZERS

Submodel	Physical model and operational constraints
	ELZ power: $P^{\text{ELZ}} = P^{\text{Rec}} + P^{\text{BoP}}$ (1)
	Rectifier power: $P^{\text{Rec}} = P^{\text{Stack}} + P^{\text{Loss}}$ , $P^{\text{Rec}} \eta^{\text{Rec}} = P^{\text{Stack}}$ (2)
	Stack power: $P^{\text{Stack}} = U^{\text{Stack}} I$ (3)
	Auxiliary power: $P^{\text{BoP}} = P^{\text{Cool}} / \eta^{\text{Cool}} + b^{\text{By}} P^{\text{By}}$ (4)
Hydrogen production	U-I characteristics: $U^{\text{Stack}} = N^{\text{Cell}} [U^{\text{rev}} + (r_1 + r_2 T) I / A + s_1 \log((t_1 + t_2 / T + t_3 / T^2) I / A + 1)]$ (5)
	Current limits: $b^{\text{On}} \bar{I} \leq I \leq b^{\text{On}} \bar{I}$ (6)
	Hydrogen flow: $Y^{\text{H}_2} = \eta^{\text{F}} N^{\text{Cell}} I / (2F)$ (7)
	Faradaic efficiency: $\eta^{\text{F}} = (I/A)^2 / [f_1 + (I/A)^2] \times f_2$ (8)
	Thermal dynamics: $C_n^{\text{ELZ}} (T_{n,t+1} - T_{n,t}) = (P_{n,t}^{\text{Heat}} - P_{n,t}^{\text{Diss}} - P_{n,t}^{\text{Cool}}) \Delta t$ (9)
Heat	Electrolytic heat: $P_{n,t}^{\text{Heat}} = P_{n,t}^{\text{Stack}} - N^{\text{Cell}} U^{\text{tn}} I_{n,t}$ (10)
	Heat dissipation: $P_{n,t}^{\text{Diss}} = (T_{n,t} - T^{\text{Am}}) / R_{n,t}^{\text{Diss}}$ (11)
	Active cooling: $P_{n,t}^{\text{Cool}} \leq (1 - b^{\text{Idle}}) c^{\text{Cool}} (T_{n,t} - T^{\text{Cool}})$ (12)
	Temperature limits: $\underline{T} \leq T_{n,t} \leq \bar{T}$ (13)
	Logical constraint: $b_{n,t}^{\text{On}} + b_{n,t}^{\text{By}} + b_{n,t}^{\text{Idle}} = 1$ (14)
State switching	Startup action: $b_{n,t}^{\text{On}} + b_{n,t}^{\text{By}} + b_{n,t}^{\text{Idle}} - 1 \leq b_{n,t}^{\text{SU}}$ (15)
	Shutdown action: $b_{n,t-1}^{\text{On}} + b_{n,t-1}^{\text{By}} + b_{n,t-1}^{\text{Idle}} - 1 \leq b_{n,t}^{\text{SD}}$ (16)
	Startup delay: $-b_{n,t-2}^{\text{Idle}} - b_{n,t-1}^{\text{Idle}} + b_{n,t-1}^{\text{Idle}} \leq 0$ (17)

Note:  $U^{\text{rev}}$  and  $U^{\text{tn}}$  are the reversible voltage and thermal neutral voltage;  $N^{\text{cell}}$  and  $A$  are the cell number and electrode area of the stack;  $r_1, r_2, s_1, t_1, t_2$  and  $t_3$  are coefficients of the U-I curve;  $F$  is the Faraday constant;  $f_1$  and  $f_2$  are the coefficients of Faradaic efficiency.

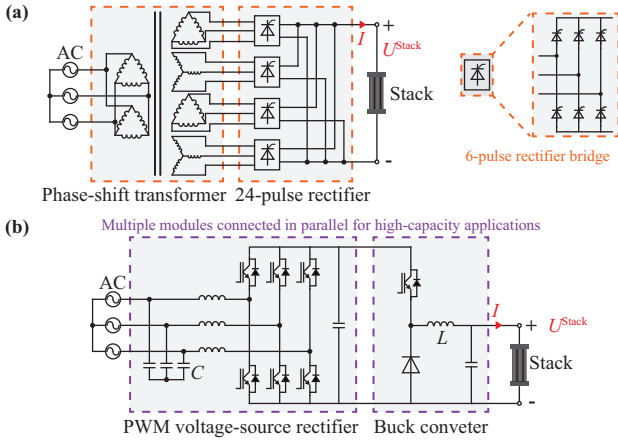


Fig. 3. The detailed topologies of (a) 24-pulse TR, and (b) IGBT-R.

$Q^{\text{TR}}$ , stack voltage  $U^{\text{Stack}}$  and AC bus voltage  $U^{\text{AC}}$  follows [6]:

$$Q^{\text{TR}} = 2.44 P^{\text{Stack}} U^{\text{AC}} / (\eta^{\text{Rec}} K^{\text{Rec}} U^{\text{Stack}}) \times \sqrt{\sin^2 \left[ \arccos \left( \frac{K^{\text{Rec}} U^{\text{Stack}}}{2.44 U^{\text{AC}}} \right) \right] + \frac{1 - \nu^2}{\nu^2}}, \quad (18)$$

where  $K^{\text{Rec}}$  is the turn ratio of the rectifier transformer and where  $\nu$  is the harmonic factor of the 24-pulse TR. Since  $P^{\text{Stack}}$  and  $U^{\text{Stack}}$  depend on  $I$  and  $T$ , substituting (3) and (5) into (18) yields the complete expression for  $Q^{\text{TR}}(U^{\text{AC}}, I, T)$ , which is used for MR configuration planning in Section III.

2) *IGBT-R*: Compared with TRs, IGBT-Rs offer more flexible reactive power characteristics. Two operational modes exist as listed below.

- *Fixed Power Factor (PF = 1)* (Industrial practices [8]): Many existing distributed control systems (DCSs) of hydrogen plants lack a built-in reactive power control interface.

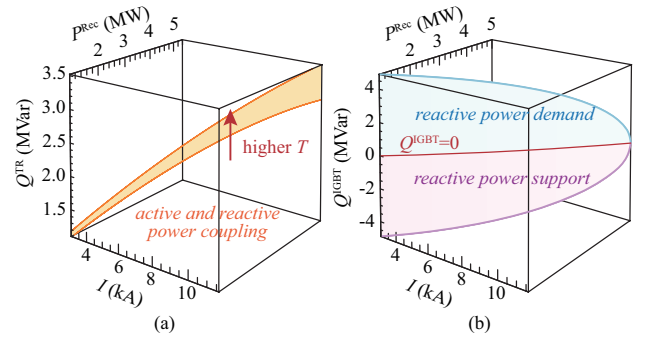


Fig. 4. The active-reactive power characteristics of ELZs powered by different rectifiers under varying electrolytic currents. (a) TR. (b) IGBT-R

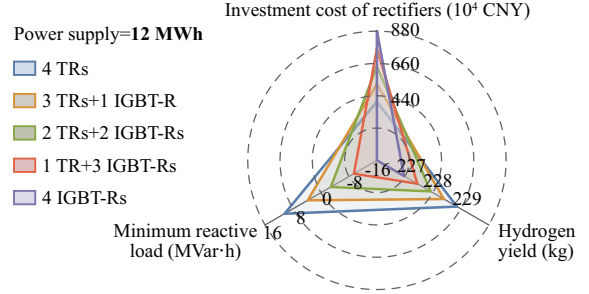


Fig. 5. Comparison of the investment cost, hydrogen productivity, and reactive demand under different rectifier configurations for 4 ELZs.

Thus, IGBT-Rs are often set to a fixed unit PF:

$$Q^{\text{IGBT}} = 0. \quad (19)$$

- *Adjustable Reactive Power* (Academia [9], [10] and industry standards [29]): IGBT-Rs can supply or absorb reactive power within capacity limits [9] to act as a compensator:

$$(P^{\text{Rec}})^2 + (Q^{\text{IGBT}})^2 \leq (S^{\text{IGBT}})^2. \quad (20)$$

3) *Comparison*: ① As shown in Fig. 3, the PWM and two-stage topology of the IGBT-R result in higher switching and conduction losses than those of the TR, leading to greater losses  $P^{\text{Loss}}$  and lower efficiency  $\eta^{\text{Rec}}$  than those of the TR. ② The IGBT-R also requires a larger plant area, increasing investment costs. ③ Figs. 4(a) and 4(b) compare the active and reactive power characteristics of the TR and IGBT-R for a 5 MW ELZ (rated flow of 1,000 Nm<sup>3</sup>/h). As shown in Fig. 4(a), the TR's active and reactive power are coupled, meaning that for a fixed electrolytic current, the reactive power remains uncontrollable, varying only within the orange region as the stack temperature changes. In contrast, Fig. 4(b) shows that the IGBT-R provides greater flexibility. For a fixed active power or current, the IGBT-R can supply reactive power (purple region), absorb reactive power (blue region), or maintain a PF of 1 (red curve).

To illustrate the impact of different rectifier configurations, a straightforward example is given. A hydrogen plant with four 5 MW ELZs supplied with 12 MW of power for one hour is considered. Using hydrogen production maximization as the objective, we calculate the hydrogen yield and reactive power demand for each configuration. Fig. 5 presents the results along with the investment costs. TRs offer lower costs and slightly higher hydrogen production, whereas IGBT-Rs provide reactive power support, which is critical for voltage security, reducing AC network losses, lowering var compensator costs,

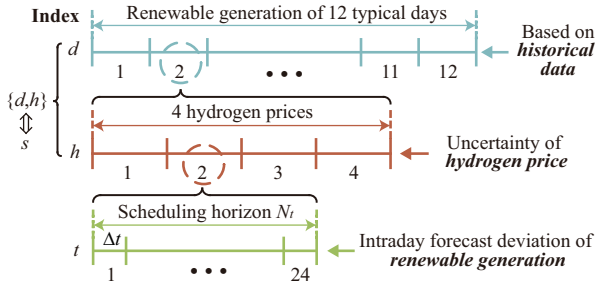


Fig. 6. Planning framework for mixed rectifiers, ELZs, and var resources. and enhancing the overall profitability of the ReP2H system, as demonstrated in our previous work [6]. An MR configuration may achieve an optimal balance among these factors.

**Remark 1.** *Although the active and reactive powers of the TR are coupled, they are both governed by the electrolytic load and temperature. Managing the load allocation and temperature of multiple TR-powered ELZs can optimize the reactive power flow in the ReP2H system to improve overall productivity; see the tradeoff emphasized in Section II-E of [6]. In other words, the investment planning and production scheduling of the hydrogen plant should be coordinated with the electrical network.*

### III. OPTIMAL INVESTMENT PORTFOLIO PLANNING OF MIXED RECTIFIER CONFIGURATIONS

#### A. Planning Framework

The planning framework consists of two stages:

- *Investment stage:* Determines the number of ELZs, type and number of rectifiers, and capacity of the static var generator (SVG) for compensation.
- *Operational stage:* Employs the coordinated active-reactive power scheduling method proposed in our prior work [6] to manage renewables, multiple ELZs, BES, and var resources.

The ReP2H system faces uncertainties [32], including the hydrogen price and renewable power over three different timescales. We address these issues using the framework in Fig. 6. First, we use 12 typical days across four seasons to represent baseline patterns of renewable power. Second, for each typical day, we use four hydrogen price scenarios [33] to describe its uncertainty. Finally, intraday wind and solar power uncertainties are handled via IGDT [34]. The intraday uncertainty is modeled as a set  $\mathcal{B}$ , which describes the uncertainty horizon  $\alpha$  on the basis of the baseline  $\tilde{P}_{s,t}^{\text{WT/PV}}$ , formulated as:

$$\mathcal{B}(\alpha, \tilde{P}_{s,t}^{\text{WT/PV}}) = \{P_{s,t}^{\text{WT/PV}} : \left| \frac{P_{s,t}^{\text{WT/PV}} - \tilde{P}_{s,t}^{\text{WT/PV}}}{\tilde{P}_{s,t}^{\text{WT/PV}}} \right| \leq \alpha\}. \quad (38)$$

where  $s$  represents the day price index  $\{d, h\}$  for simplicity.

#### B. Objective Function

The objective of the MR investment portfolio model is to maximize the total revenue  $J^{\text{Tot}}$ :

$$\max J^{\text{Tot}} = J^{\text{Inv}} + J^{\text{Ope}}, \quad (39)$$

where the investment cost  $J^{\text{Inv}}$  covers ELZs, rectifiers, and var resources, as

$$J^{\text{Inv}} = -r(1+r)^y / [(1+r)^y - 1] \times (c^{\text{C}}W^{\text{C}} + c^{\text{TR}}\sigma^{\text{TR}} + c^{\text{IGBT}}\sigma^{\text{IGBT}} + c^{\text{ELZ}}\sigma^{\text{ELZ}}), \quad (40)$$

and the operational revenue  $J^{\text{Ope}}$  considers hydrogen production and sale revenues, startup/shutdown costs of ELZs, and operation and maintenance (O&M) costs, i.e.,

$$J^{\text{Ope}} = 365 \sum_{s=1}^{N_s} \pi_s J_s^{\text{Ope}}, \quad (41)$$

$$J_s^{\text{Ope}} = \sum_{t=1}^{N_t} \sum_{n=1}^{\sigma^{\text{ELZ}}} (c^{\text{H}_2} Y_{n,t}^{\text{H}_2} - c^{\text{SU}} b_{n,t}^{\text{SU}} - c^{\text{SD}} b_{n,t}^{\text{SD}}) + \frac{\eta_{\text{O\&M}} J^{\text{Inv}}}{365}. \quad (42)$$

Here,  $r$  and  $y$  are the discount rate and equipment lifespan, respectively;  $\pi_s$  represents the probability of scenario  $s$ ; and  $\eta_{\text{O\&M}} = 2\%$  is the annual O&M cost factor.

#### C. Investment and Operational Constraints

1) *Investment constraints:* Constrained by available land, the number of ELZs satisfies (43), and the number of rectifiers must match the ELZs, following (44). To ensure the electrical strength of the AC system, the short-circuit ratio  $R^{\text{sc}}$  at the hydrogen plant must exceed a threshold [35]. TRs rely on grid support for reliable commutation, requiring high  $R^{\text{sc}}$ , whereas IGBT-Rs can provide support to the AC grid [10], [11], reducing the requirement for  $R^{\text{sc}}$ . Thus,  $R^{\text{sc}}$  is estimated as (45) for a fast assessment of electrical strength.

$$0 \leq \sigma^{\text{ELZ}} \leq \bar{\sigma}^{\text{ELZ}}, \quad (43)$$

$$\sigma^{\text{TR}} + \sigma^{\text{IGBT}} = \sigma^{\text{ELZ}}, \quad (44)$$

$$R^{\text{sc}} = \frac{S^{\text{sc}}}{(\sigma^{\text{TR}} S^{\text{TR}} + \sigma^{\text{IGBT}} S^{\text{IGBT}})} \geq \frac{3\sigma^{\text{TR}} + 2\sigma^{\text{IGBT}}}{\sigma^{\text{TR}} + \sigma^{\text{IGBT}}}. \quad (45)$$

Note that the electrical strength is roughly evaluated here for investment planning. An accurate assessment of the strength and threshold of the short-circuit ratio in ReP2H systems requires electromagnetic analysis and should be explored in future work.

2) *Operational constraints:* We consider the coordination among active and reactive resources such as the electrical network, ELZs, WTs, PV plants, BES, var compensation, and OLTC. Their models are presented in Table III, where we use the DistFlow model [30] to describe the network power flow, which is radial in common ReP2H systems.

In operation, active power balance is achieved by on-off switching and load allocation among multiple ELZs in the hydrogen plant, assisted by the BES. The reactive power flow is optimized in coordination with the active power to support the voltage and reduce network losses. The OLTC regulates the voltage at the hydrogen plant to ensure that the TR firing angle stays within a preferred range. For details of the operation model, readers are referred to [6].

#### D. The Overall Optimal Portfolio Model

1) *Planning with  $\alpha = 0$ :* As per the IGDT procedure, first, we assume zero intraday uncertainty for the wind and solar power in typical-day scenarios. The optimal portfolio model for the MR configuration is given as follows:

$$\bar{J}^{\text{Tot}} = \max (39), \quad (46a)$$

$$\text{s.t. (1)-(17), (18), (19) or (20), (21)-(37), (43),} \quad (46b)$$

where  $\bar{J}^{\text{Tot}}$  is the total revenue. We denote the investment cost as  $\bar{J}^{\text{Inv}}$  and the operational revenue under scenario  $s$  as  $\bar{J}_s^{\text{Ope}}$ .



TABLE III  
MODEL AND OPERATIONAL CONSTRAINTS OF THE AC NETWORK IN THE REP2H SYSTEM

Operational constraints		
Power flow [30]	Branch active power injections: $\sum_{j' \in \sigma(j)} P_{jj',t} = p_{j,t} + \sum_{i \in \pi(j)} P_{ij,t} - r_{ij} l_{ij,t}$ (21)	
	Branch reactive power injections: $\sum_{j' \in \sigma(j)} Q_{jj',t} = q_{j,t} + \sum_{i \in \pi(j)} Q_{ij,t} - x_{ij} l_{ij,t}$ (22)	
	Ohm's law of transmission line: $v_{j,t} = v_{i,t} - 2(r_{ij} P_{ij,t} + x_{ij} Q_{ij,t}) + (r_{ij}^2 + x_{ij}^2) l_{ij,t}$ (23)	
	Ohm's law of transformer branch: $\sum_{k=0}^{K_{ij}} (w_{ij,k})^2 \delta_{ij,k,t} v_{j,t} = v_{i,t} - 2(r_{ij} P_{ij,t} + x_{ij} Q_{ij,t}) + (r_{ij}^2 + x_{ij}^2) l_{ij,t}$ (24)	
	Second-order cone relaxation: $\ (2P_{ij,t}, 2Q_{ij,t}, l_{ij,t} - v_{i,t})\ _2 \leq l_{ij,t} + v_{i,t}$ (25)	
	Auxiliary variables for squared voltage and current and security constraints: $\underline{U}_j^2 \leq v_{j,t} =  U_{j,t} ^2 \leq \bar{U}_j^2, l_{ij,t} =  I_{ij,t} ^2 \leq \bar{I}_{ij}^2$ (26)	
	Bus injected power: $p_{j,t} = P_{j,t}^{\text{WT}} + P_{j,t}^{\text{PV}} - P_{j,t}^{\text{BES,C}} + P_{j,t}^{\text{BES,D}} - P_{j,t}^{\text{L}}, q_{j,t} = Q_{j,t}^{\text{WT}} + Q_{j,t}^{\text{PV}} - Q_{j,t}^{\text{BES,C}} + Q_{j,t}^{\text{BES,D}} - Q_{j,t}^{\text{L}}$ (27)	
	Power of hydrogen plant: $p_{j,t}^{\text{L}} = \sum_{n=1}^{\sigma_{\text{ELZ}}} P_{n,t}^{\text{ELZ}}, q_{j,t}^{\text{L}} = \sum_{n=1}^{\sigma_{\text{TR}}} Q_{n,t}^{\text{TR}} + \sum_{n=1}^{\sigma_{\text{IGBT}}} Q_{n,t}^{\text{IGBT}}$ (28)	
	WTs and PV plants [6]	Reactive power of WTs: $1.24P_{j,t}^{\text{WT}} - 0.91S_{j,t}^{\text{WT}} \leq Q_{j,t}^{\text{WT}} \leq 0.91S_{j,t}^{\text{WT}} - 0.58P_{j,t}^{\text{WT}}$ (29)
		Reactive power of PV plants: $(P_{j,t}^{\text{PV}})^2 + (Q_{j,t}^{\text{PV}})^2 \leq (S_{j,t}^{\text{PV}})^2, -P_{j,t}^{\text{PV}} \tan \theta \leq Q_{j,t}^{\text{PV}} \leq P_{j,t}^{\text{PV}} \tan \theta$ (30)
BES [31]	Active and reactive power of BES: $(P_{j,t}^{\text{BES,CD}})^2 + (Q_{j,t}^{\text{BES}})^2 \leq (S_{j,t}^{\text{BES}})^2$ (31)	
	Charge and discharge: $0 \leq P_{j,t}^{\text{BES,CD}} \leq b_{j,t}^{\text{BES,CD}}, b_{j,t}^{\text{BES,C}} + b_{j,t}^{\text{BES,D}} \leq 1$ (32)	
	State of charge of BES: $E_{j,t+1} = (1 - \zeta^{\text{BES}}) E_{j,t} + (\eta^{\text{BES,C}} P_{j,t}^{\text{BES,C}} - P_{j,t}^{\text{BES,D}} / \eta^{\text{BES,D}}) \Delta t$ (33)	
	State of charge constraints: $E_{j,t=0} = E_{j,t=N_t}, \underline{E} \leq E_{j,t} \leq \bar{E}$ (34)	
Var compensation	Reactive power of var compensation: $-W^{\text{C}} \leq Q_{j,t}^{\text{C}} \leq W^{\text{C}}$ (35)	
OLTC [6]	OLTC tap position modeling: $k_{ij,t} = \sum_{k=0}^{K_{ij}} \delta_{ij,k,t} w_{ij,k}, \sum_{k=0}^{K_{ij}} \delta_{ij,k,t} = 1, \delta_{ij,k,t} \in \{0, 1\}$ (36)	
	Action and operational range constraints: $\sum_{t=2}^{N_t}  k_{ij,t} - k_{ij,t-1}  \leq \bar{k}_{ij}^{\text{All}}, \underline{k}_{ij} \leq k_{ij,t} \leq \bar{k}_{ij}$ (37)	

2) *W-IGDT-based portfolio model*: To handle the intraday uncertainty of renewable power, a risk-averse model based on robust IGDT [34] is developed. Based on the revenue of (46), with a preset deviation factor  $\beta > 0$ , the robust IGDT model maximizes the uncertainty boundary  $\alpha$  under the worst-case renewable generation, as follows:

$$\max \alpha \quad (47a)$$

$$\text{s.t. } J^{\text{Tot}} \geq (1 - \beta) \tilde{J}^{\text{Tot}}, \quad (47b)$$

$$P_{s,t}^{\text{WT/PV}} = (1 - \alpha) \tilde{P}_{s,t}^{\text{WT/PV}}, \quad \forall s \quad (47c)$$

$$(46b). \quad (47d)$$

Since higher renewable penetration corresponds to higher risk, scenarios with higher renewable power output require larger uncertainty boundaries to mitigate the risk [36]. Therefore, we assign weights to the boundaries  $\alpha_s$  on the basis of power output levels for different scenarios, improving the conventional IGDT model to the W-IGDT [36] model to better manage the risk. The W-IGDT version of (47) is as follows:

$$\max \sum_s \pi_s \frac{N_s \sum_t (\tilde{P}_{s,t}^{\text{WT}} + \tilde{P}_{s,t}^{\text{PV}})}{\sum_s \sum_t (\tilde{P}_{s,t}^{\text{WT}} + \tilde{P}_{s,t}^{\text{PV}})} \alpha_s, \quad (48a)$$

$$\text{s.t. } J^{\text{Inv}} + 365 J_s^{\text{Ope}} \geq (1 - \beta) (J^{\text{Inv}} + 365 \tilde{J}_s^{\text{Ope}}), \quad \forall s, \quad (48b)$$

$$P_{s,t}^{\text{WT/PV}} = (1 - \alpha_s) \tilde{P}_{s,t}^{\text{WT/PV}}, \quad \forall s, \quad (48c)$$

$$(46b). \quad (48d)$$

### E. Two-stage Decomposition-Based Solution Approach—PH

The established optimal portfolio model (46) uses mixed-integer nonlinear programming (MINLP), which is difficult to solve. Therefore, we use polynomial approximation, piecewise linearization, and the Big-M method to transform it into mixed-integer second-order cone programming (MISOCP). Nevertheless, the reformulated model is large in scale, involves various active and reactive power resources, and requires multiple scenarios to address uncertainty. Specifically, for an 8-node small-scale system with 4 ELZs (in Section IV-A-1), the model has

358,512 constraints, 167,328 continuous variables, and 42,624 binary variables. This makes direct solving infeasible, akin to large-scale systems.

Fortunately, the proposed model is a standard two-stage SP, with each stage presenting investment or operation. Therefore, we can adopt the PH algorithm [25], which is effective for accelerating the solution of the SP. We decompose the SP into  $N_s$  subproblems, compactly expressed as:

$$\min_{\{\mathbf{x}, \mathbf{y}_s, \forall s\}} \mathbf{a}^T \mathbf{x} + \sum_{s=1}^{N_s} \pi_s \mathbf{b}_s^T \mathbf{y}_s \quad (49)$$

$$\text{s.t. } \mathbf{x} \in X, \mathbf{y}_s \in Y_s, \forall s \quad (50)$$

where  $\mathbf{a}$  and  $\mathbf{b}_s$  are coefficient matrices;  $\mathbf{x}$  and  $\mathbf{y}_s$  are the vectors of investment and operational variables, respectively, with  $X$  and  $Y_s$  as their feasible sets. Then, we can use Algorithm 1 to solve the portfolio model effectively by solving the investment and operational variables iteratively.

## IV. CASE STUDIES

Case studies are performed on two real-world systems in Inner Mongolia, China, as shown in Fig. 7. The test systems are adapted from our prior work [6]. The small-scale system validates the proposed portfolio model and explores the potential of MR configurations, whereas the large-scale system verifies the scalability of the model and provides insights for practice. Simulations are performed via *Wolfram Mathematica 14.0*, with optimizations solved via *Gurobi 11.0.0*.

### A. Test System Settings

1) *Small-scale system*: The system consists of  $3 \times 6.25$  MW WTs at buses 1-3, a 5 MW PV plant at bus 4, and a 2 MW/4 MWh BES at bus 7. The investment decisions involve the number of ELZs and rectifiers at the hydrogen plant at the bus and the SVG capacity at bus 6.

**Algorithm 1** PH Algorithm for the Portfolio Model

- 1: **precondition:** Initialize the iteration index  $m \leftarrow 0$ , Lagrange multiplier  $\omega_s^0 \leftarrow 0$  and convergence index  $g^0$ , and select the convergence tolerance  $\epsilon \leftarrow 10^{-3}$
- 2: Get the investment and operational variables in parallel by  $\{\mathbf{x}_s^0, \mathbf{y}_s^0\} \leftarrow \arg \min_{\{\mathbf{x}, \mathbf{y}_s\}} \{\mathbf{a}^T \mathbf{x} + \sum_s \mathbf{b}_s^T \mathbf{y}_s : (50)\}$  for  $\forall s$
- 3: Calculate the initial value for the investment variable  $\bar{\mathbf{x}}^0 \leftarrow \sum_s \pi_s \mathbf{x}_s^0$
- 4: **while**  $g^m \leq \epsilon$  **do**
- 5:   **for**  $s = 1$  **to**  $N_s$  **do**
- 6:     Update the index  $m \leftarrow m + 1$ , and multiplier  $\omega_s^m \leftarrow \omega_s^{m-1} + \rho(\mathbf{x}_s^{m-1} - \bar{\mathbf{x}}^{m-1})$
- 7:     Update the investment and operational variables  $\{\mathbf{x}_s^m, \mathbf{y}_s^m\} \leftarrow \arg \min_{\{\mathbf{x}, \mathbf{y}_s\}} \{\mathbf{a}^T \mathbf{x} + \mathbf{b}_s^T \mathbf{y}_s + (\omega_s^m)^T \mathbf{x} + \rho/2 \|\mathbf{x} - \bar{\mathbf{x}}^{m-1}\|^2 : (50)\}$
- 8:   **end for**
- 9:   Calculate the investment solution  $\bar{\mathbf{x}}^m \leftarrow \sum_s \pi_s \mathbf{x}_s^m$
- 10:   Assess the convergence  $g^m \leftarrow \sum_s \pi_s \|\mathbf{x}_s^m - \bar{\mathbf{x}}^m\|_2$
- 11: **end while**
- 12: **return**  $(\bar{\mathbf{x}}^m, \mathbf{y}_1^m, \dots, \mathbf{y}_{N_s}^m)$

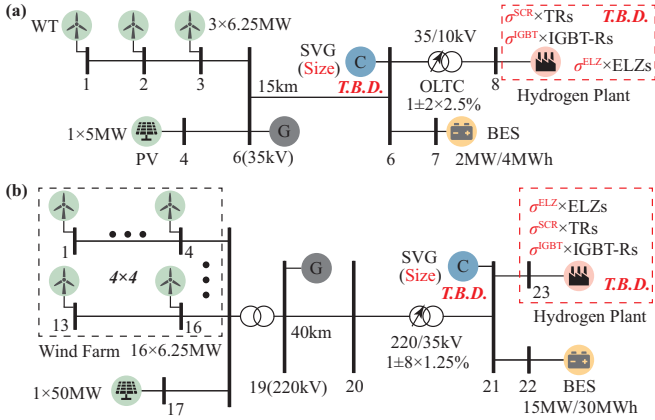


Fig. 7. Topologies of the ReP2H systems used for the case study. (a) Small-scale system with 23.75 MW of renewable energy. (b) Large-scale system with 150 MW of renewable energy.

2) *Large-scale system:* Includes 16×6.25 MW WTs, 1×50 MW PV plant, 1×15 MW/30 MWh BES. The hydrogen plant and SVG are located at buses 21 and 23, respectively.

The key investment parameters are listed in Table IV. The topology and operational details of the ReP2H system and ELZs are available in [6]. Renewable generation for typical days, derived from on-site historical data via K-means clustering, is shown in Figs. 8(a) and 8(b). The hydrogen price scenario is shown in Fig. 8(c), with fluctuations modeled based on local agricultural ammonia demand [32].

### B. Investment Portfolio Results of the Small-scale System for $\beta = 0$ ( $\alpha = 0$ )

For the small-scale system, with the intraday renewable power uncertainty set to zero, the rectifier configurations of four ELZs

TABLE IV  
THE KEY INVESTMENT PARAMETERS FOR CASE STUDIES

Facility	Rating	Unit investment cost	Discount rate $r$	Lifetime $y$
ELZ w/o rectifier	5 MW	7,000,000 CNY	8%	20 years
TR	6 MVA	1,000,000 CNY		
IGBT-R	6 MVA	2,200,000 CNY		
SVG		350 CNY/kVar		

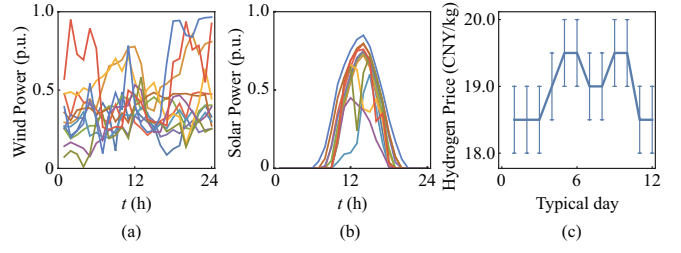


Fig. 8. Scenarios of wind and solar power generation and the average hydrogen price of 12 typical days. (a) Wind power. (b) Solar power. (c) Hydrogen price.

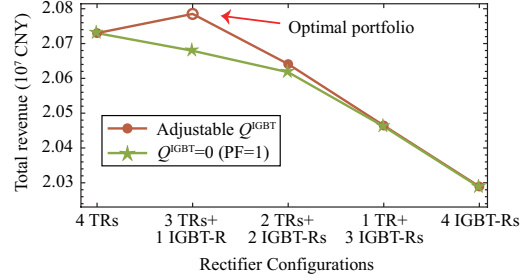


Fig. 9. Total revenue of different rectifier configurations.

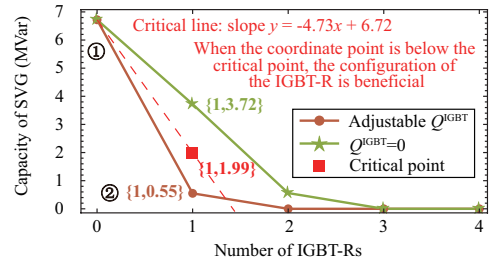


Fig. 10. The optimal SVG capacity under varying numbers of IGBT-Rs.

are evaluated. Fig. 9 presents the total revenues of different portfolios of TR and IGBT-R, while Table V summarizes the planning and operational results. Among the results, cases where IGBT-Rs are allowed to adjust reactive power are denoted ②-⑤, and cases where the PF of the IGBT-R is fixed at 1 are denoted ⑥-⑨ (see the discussion about reactive power characteristics in Section II-C-2).

As shown in Fig. 9, when the IGBT-Rs are allowed to provide reactive power, the optimal configuration is 3 TRs and 1 IGBT-R. In contrast, if the IGBT-R is fixed at PF = 1, a uniform configuration of 4 TRs is preferable. The reasons are as follows.

Comparing ① and ⑥, we find that while 1 IGBT-R at PF = 1 reduces the need for 4 MVar of SVG, it does not offset its higher cost and lower efficiency, leading to reduced hydrogen yield. Consequently, under configurations ⑥-⑨, IGBT-Rs with PF = 1 are less cost-effective than TRs are. By further comparing ① and ②, we find that IGBT-Rs with adjustable reactive power support reduce SVG investment, resulting in lower overall costs for rectifiers and var compensation (①:  $100 \times 4 + 35 \times 6.72 = 635.2 \times 10^4$  CNY, ②:  $100 \times 3 + 220 \times 1 + 35 \times 0.55 = 539.25 \times 10^4$  CNY), resulting in optimal returns.

In terms of hydrogen production in configurations ① to ⑨, Table V shows that each additional IGBT-R reduces the hydrogen yield by approximately 2,500 kg/year, resulting in an estimated decrease in revenue of  $4.75 \times 10^4$  CNY. On the other hand, the annual cost of an IGBT-R is  $0.104 \times (220 - 100) = 12.48 \times 10^4$  CNY greater than that of a TR considering the discount. Therefore, an IGBT-R investment is justified only if it reduces SVG capacity by at least  $(12.48 + 4.75) / (0.104 \times 35) =$

TABLE V  
PLANNING AND OPERATIONAL RESULTS UNDER DIFFERENT RECTIFIER CONFIGURATIONS IN THE 4-ELZ SYSTEM

Configuration (TR + IGBT-R)	Total Revenue ( $10^7$ CNY/yr)	SVG Capacity (MVar)	Hydrogen Yield ( $10^5$ kg/yr)	Network loss (MWh/yr)
① 4 + 0	2.0730	6.72	<b>1362.64</b>	1233.1
② 3 + 1	<b>2.0785</b>	0.55	1360.27	1229.3
③ 2 + 2	2.0641	0	1358.21	1218.0
④ 1 + 3	2.0465	0	1355.46	1217.8
⑤ 0 + 4	2.0289	0	1352.77	<b>1211.8</b>
⑥ 3 + 1	2.0679	3.72	1360.77	1238.3
⑦ 2 + 2	2.0618	0.56	1358.09	1235.5
⑧ 1 + 3	2.0462	0	1355.32	1228.0
⑨ 0 + 4	2.0288	0	1352.68	1217.9

\* IGBT-R provides reactive power in ②-⑤ and operates at PF = 1 in ⑥-⑨.

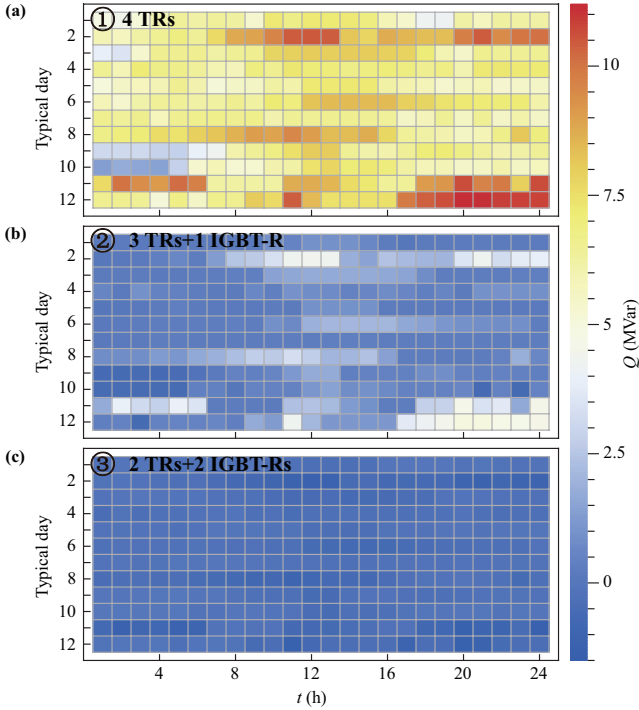


Fig. 11. Reactive power demand of the hydrogen plant with different rectifier configurations under 12 scenarios in the first representative year. (a) ① 4 TRs. (b) ② 3 TRs + 1 IGBT-R. (c) ③ 2 TRs + 2 IGBT-Rs.

4.73 MVar. In particular, Fig. 10 shows the SVG capacity with varying numbers of IGBT-Rs, along with the critical point at which configuring more IGBT-Rs is beneficial. It is clear that the only case ①→② meets the conditions.

### C. Operational Analysis of Different Rectifier Configurations

To analyze the operational differences of the ReP2H system under various rectifier configurations, we focus on configurations ①-③. Configurations ④ and ⑤ are similar to ③, whereas ⑥-⑨ lack economic advantages and are thus left out here. The total reactive power demand of the hydrogen plant under different configurations and typical days (for a single hydrogen price scenario) is shown in Fig. 11. The electrolytic load and reactive power of the four ELZs in a typical renewable generation scenario under configurations ①-③ are illustrated in Figs. 12 to 14, respectively.

Fig. 11 shows that a hydrogen plant powered by four TRs exhibits significant reactive power demand (over 6 MVar) across most scenarios. In contrast, replacing one TR with an IGBT-R can reduce the reactive power demand to below 1.5 MVar,

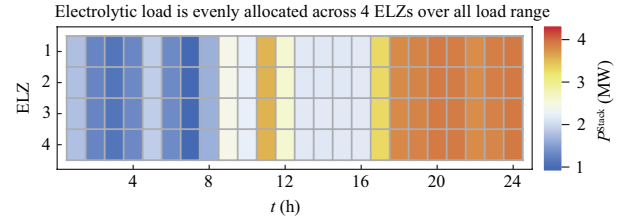


Fig. 12. Electrolytic load of 4 ELZs in the typical renewable generation scenario under configuration ① with 4 TRs.

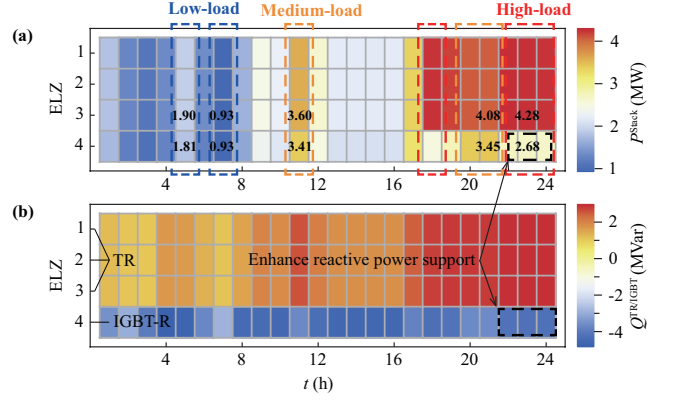


Fig. 13. (a) DC-side electrolytic load and (b) AC-side reactive power of 4 ELZs in the typical scenario under the optimal configuration ② with 3 TRs and 1 IGBT-R.

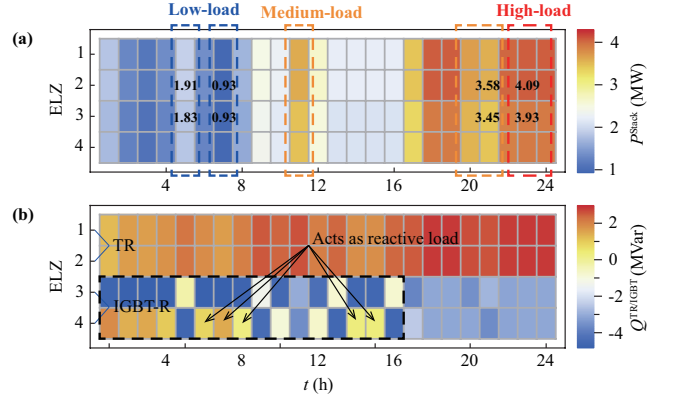


Fig. 14. (a) DC-side electrolytic load and (b) AC-side reactive power of 4 ELZs in the typical scenario under configuration ③ with 2 TRs and 2 IGBT-Rs.

achieving local balance and reducing the reactive power flow and network losses. Configuration ③ with 2 TRs and 2 IGBT-Rs provides reactive power support of approximately 0–0.6 MVar to the network. Clearly, this configuration has excessive var resources, making it less cost-effective.

As shown in Fig. 12, when the rectifiers in all ELZs are uniform and var resources are adequate, the electrolytic load is evenly distributed across the ELZs to maximize the hydrogen yield, aligning with the equimarginal principle and resulting in [6]. In contrast, mixed rectifier configurations ② and ③, as shown in Figs. 13 and 14, result in ELZs powered by TRs bearing a slightly higher load than those powered by IGBT-Rs in ② and ③.

Fig. 13(a) shows that the load difference between the TR- and IGBT-powered ELZs is the smallest at low-load intervals, increases at medium-load intervals, and peaks at high-load intervals. Combining Fig. 13(b), we see that reducing the load of IGBT-powered ELZs releases their reactive support capability (see Fig. 4(b)), facilitating local reactive power balance at the



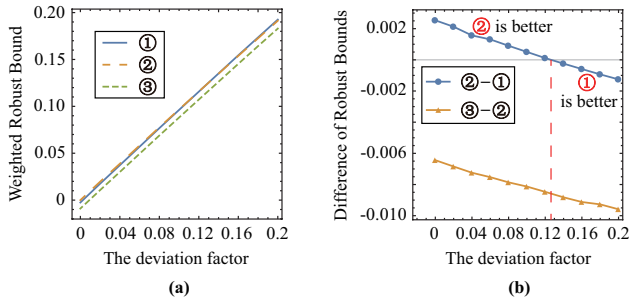


Fig. 15. Weighted robust uncertainty bounds of different  $\beta$  under configurations ① 4 TRs, ② 3 TRs + 1 IGBT-R and ③ 2 TRs + 2 IGBT-Rs, and the differences among them. (a) Robust bound. (b) Difference.

hydrogen plant at high loads, minimizing network losses, and ensuring voltage stability. However, the concentrating load in a few ELZs lowers the overall P2H energy conversion efficiency, as dictated by the electrochemical characteristics (Section II-B) and the equimarginal principle [6], [37]. Thus, during low- and medium-load intervals, when the reactive power demand is lower, a more even load distribution improves the hydrogen yield. Furthermore, Fig. 14(b) shows that at low- and medium-load intervals, the IGBT-R even acts as a reactive load, confirming a surplus in var resources in configuration ③ (2 TRs, 2 IGBT-Rs).

#### D. Robust Portfolio Results of the Small-scale System for $\beta > 0$

With four ELZs and a revenue deviation factor  $\beta$  ranging from 0 to 0.2, Fig. 15(a) presents the maximum weighted robust uncertainty bounds for different configurations, whereas Fig. 15(b) illustrates the differences among them.

As depicted in Fig. 15(a), decreasing  $\beta$  increases both the robust bound and the acceptable risk. In managing renewable generation uncertainty, configurations ① and ② perform similarly and outperform ③. Fig. 15(b) further shows that as  $\beta$  increases, the advantage of configuration ② over ① diminishes. This is because the reduced renewable output relaxes the network power flow constraints, leading to a reduction in the reactive power demand. When  $\beta > 0.12$ , configuration ① outperforms ②. This demonstrates that under high uncertainty risk, the IGDT model provides better results than approaches that do not consider intraday uncertainties. With respect to the rectifier configuration, a higher level of renewable output and a higher proportion of stressed operations increase the demand for IGBT-Rs, whereas a lower output level favors TRs.

#### E. Application in a Large-Scale System

Finally, to verify scalability and practical applicability, we apply the proposed model to the large-scale system briefly described in Section IV-A2. A 4-in-1 ELZ configuration is adopted, where four ELZs share a set of BoPs (e.g., lye-gas separators, lye circulation loops, and purification units) to reduce the footprint and cost [38], [39]. Thus, the production-standby-idle states and temperature dynamics of each 4-in-1 unit are coupled, while the active and reactive powers remain independently scheduled.

For a deviation factor  $\beta \in [0, 0.06]$ , the optimal rectifier portfolio consists of 24 ELZs powered by 19 TRs and 5 IGBT-Rs, shown in Fig. 16. Notably, the positioning of TRs and IGBT-Rs within the 4-in-1 ELZs, i.e., whether uniform or mixed, is not optimized here and will be explored in future work.

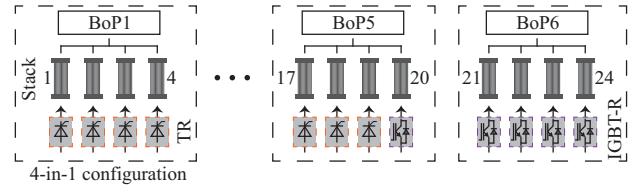


Fig. 16. Detailed configurations of the 24 ELZs in the large-scale system.

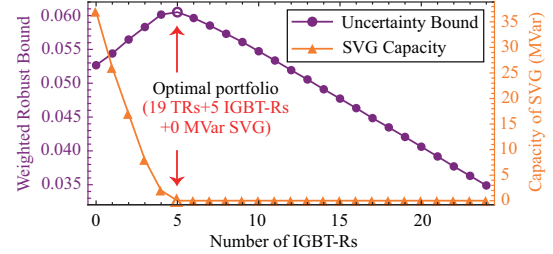


Fig. 17. Weighted robust uncertainty bounds and optimal SVG capacities of different rectifier configurations in the large-scale system for  $\beta = 0.06$ .

Table VI compares the total revenue for the optimal rectifier configuration, uniform TR/IGBT-R configurations, and ratios used in existing projects for  $\beta = 0$ . Compared with the uniform configurations, the optimal configuration increases total revenue by 0.89% to 2.56%, as well as 0.79%, 1.37%, compared with the 1:1 (32 TRs + 32 IGBT-Rs in the Da'an Project [14]) and 1:2 (12 TRs + 24 IGBT-Rs in the Songyuan Project [13]) configurations. The suboptimal portfolio (18 TRs, 6 IGBT-Rs) achieves nearly identical revenue to the optimal portfolio.

Fig. 17 displays the robust results for  $\beta = 0.06$  under different rectifier configurations. The optimal SVG capacity remains 0 MVar, which is consistent with  $\beta = 0$ , but the suboptimal configuration shifts to 20 TRs and 4 IGBT-Rs. This further confirms that IGBT-R performs better in stressed scenarios, with the full load hours of renewable energy or ELZs being key factors influencing the TR/IGBT-R ratio.

From Tables V and VI and Fig. 17, we can summarize that the optimality criterion for MR configurations can be understood as balancing the reactive power in the hydrogen plant, optimizing the investment in SVG to approximately 0, or fully utilizing the reactive power support capability of IGBT-Rs. Excessive investment in IGBT-Rs leads to idle var resources and reduced profitability. Moreover, for low renewable uncertainty, a portfolio of 18 TRs and 6 IGBT-Rs remains near-optimal. Thus, we conclude that the ideal TR-to-IGBT-R ratio for electrolysis rectifiers is approximately 3:1.

## V. CONCLUSIONS

This paper examines the complementarity of TR and IGBT-R in powering electrolyzers within ReP2H systems, explores the feasibility of mixed rectifier configurations, and integrates them into an investment planning framework. An optimal portfolio planning model and its solution approach are proposed. Simulations based on real-world systems in Inner Mongolia, China, yield the following key findings:

1) In the optimal portfolio, the reactive power support capability of the IGBT-Rs must be fully utilized, while the need for var compensation approaches zero.

2) The ideal TR-to-IGBT-R ratio for electrolysis rectifiers in ReP2H systems is approximately 3:1.

TABLE VI

COMPARISON BETWEEN DIFFERENT RECTIFIER CONFIGURATIONS IN THE LARGE-SCALE SYSTEM FOR  $\beta = 0$ 

Configuration	Total Revenue ( $10^8$ CNY/yr)	SVG Capacity (MVar)	Comparison
24 TRs (uniform)	1.2248	44	<b>+0.89%</b>
18 TRs + 6 IGBT-Rs (3:1)	1.2357	0	$\approx 0$
12 TRs + 12 IGBT-Rs (1:1)	1.2261	0	<b>+0.79%</b>
8 TRs + 16 IGBT-Rs (1:2)	1.2191	0	<b>+1.37%</b>
24 IGBT-Rs (uniform)	1.2049	0	<b>+2.56%</b>
19 TRs + 5 IGBT-Rs (optimal)	<b>1.2358</b>	0	

3) The renewable energy profile influences the rectifier portfolio, as it determines the network power flow stress. A higher proportion of stressed operations increases the demand for IGBT-Rs, whereas a lower proportion favors TRs.

Future research will focus on the transient behavior and performance of different electrolysis rectifiers, as well as their interactive mechanisms, to enhance the strength and operational stability of ReP2H systems, particularly under weak or off-grid conditions.

## REFERENCES

- [1] S. Van Renssen, "The hydrogen solution?" *Nature Clim. Chang.*, vol. 10, no. 9, pp. 799–801, 2020.
- [2] Y. Guo, et al., "Deploying green hydrogen to decarbonize China's coal chemical sector," *Nature Commun.*, vol. 14, no. 1, p. 8104, 2023.
- [3] A. Odenweller, F. Ueckerdt, G. F. Nemet, M. Jensterle, and G. Luderer, "Probabilistic feasibility space of scaling up green hydrogen supply," *Nature Energy*, vol. 7, no. 9, pp. 854–865, 2022.
- [4] The Energy Bureau of Inner Mongolia Autonomous Region, "Notice of Inner Mongolia Autonomous Region Energy Bureau on carrying out the 2022 wind-solar hydrogen production integration demonstration." [Online]. Available: <http://dbnyb.com/07/taiyangnen/2021/0827/51472.html>
- [5] Y. Qiu, et al., "Extended load flexibility of utility-scale P2H plants: Optimal production scheduling considering dynamic thermal and HTO impurity effects," *Renewable Energy*, vol. 217, p. 119198, Nov. 2023.
- [6] Y. Zeng, Y. Qiu, J. Zhu, S. Chen, B. Zhou, J. Li, B. Yang, and J. Lin, "Scheduling multiple industrial electrolyzers in renewable P2H systems: A coordinated active-reactive power management method," *IEEE Trans. Sustain. Energy*, vol. 16, no. 1, pp. 201–215, Jan. 2025.
- [7] B. Yodwong, D. Guilbert, M. Phattanasak, W. Kaewmanee, M. Hinaje, and G. Vitale, "AC-DC converters for electrolyzer applications: State of the art and future challenges," *Electronics*, vol. 9, no. 6, p. 912, May 2020.
- [8] J. Koponen, et al. "Comparison of thyristor and insulated-gate bipolar transistor-based power supply topologies in industrial water electrolysis applications," *J. Power Sources*, vol. 491, p. 229443, Apr. 2021.
- [9] A. M. De Corato, M. Ghazavi Dozein, S. Riaz, et al., "Hydrogen electrolyzer load modelling for steady-state power system studies," *IEEE Trans. Power Deliv.*, vol. 38, no. 6, pp. 4312–4323, Dec. 2023.
- [10] M. Zhang, et al., "Research on low voltage ride through and reactive power support of hydrogen production power supply," in *2022 4th Int. Conf. Smart Power & Internet Energy Syst.* IEEE, 2022, pp. 438–442.
- [11] S. D. Tavakoli, et al., "Grid-forming services from hydrogen electrolyzers," *IEEE Trans. Sustain. Energy*, vol. 14, no. 4, pp. 2205–2219, Oct. 2023.
- [12] V. Ruuskanen, J. Koponen, A. Kosonen, M. Niemelä, J. Ahola, and A. Hämäläinen, "Power quality and reactive power of water electrolyzers supplied with thyristor converters," *J. Power Sources*, vol. 459, p. 228075, May 2020.
- [13] China Energy Engineering, "China Energy Engineering's Songyuan hydrogen industry park," [http://www.ceehe.ceec.net.cn/art/2023/9/26/art\\_59190\\_802.html](http://www.ceehe.ceec.net.cn/art/2023/9/26/art_59190_802.html), 2023.
- [14] Da'an Municipal People's Government, "Da'an integrated green hydrogen and ammonia demonstration project: Building momentum for a green future," 2024. [Online]. Available: [http://daan.jlbc.gov.cn/daxw/ztbd/202410/t20241007\\_1000080.html](http://daan.jlbc.gov.cn/daxw/ztbd/202410/t20241007_1000080.html)
- [15] J. Li, B. Yang, J. Lin, F. Liu, Y. Qiu, Y. Xu, R. Qi, and Y. Song, "Two-layer energy management strategy for grid-integrated multi-stack power-to-hydrogen station," *Appl. Energy*, vol. 367, p. 123413, Aug. 2024.
- [16] Y. Gao, X. Wang, and X. Meng, "Advanced rectifier technologies for electrolysis-based hydrogen production: A comparative study and real-world applications," *Energies*, vol. 18, no. 1, p. 48, Dec. 2024.
- [17] Intellipower, "Harmonic analysis and solutions for large-scale water electrolysis hydrogen production," 2022. [Online]. Available: <https://www.intellipower.cn/industry-735>
- [18] J. Li, J. Lin, H. Zhang, Y. Song, G. Chen, L. Ding, and D. Liang, "Optimal investment of electrolyzers and seasonal storages in hydrogen supply chains incorporated with renewable electric networks," *IEEE Trans. Sustain. Energy*, vol. 11, no. 3, pp. 1773–1784, Jul. 2020.
- [19] G. Pan, W. Gu, Y. Lu, H. Qiu, S. Lu, and S. Yao, "Optimal planning for electricity-hydrogen integrated energy system considering power to hydrogen and heat and seasonal storage," *IEEE Trans. Sustain. Energy*, vol. 11, no. 4, pp. 2662–2676, Oct. 2020.
- [20] J. Zhu, Y. Qiu, Y. Zeng, et al., "Exploring the optimal size of grid-forming energy storage in an off-grid renewable P2H system under multi-timescale energy management," *arXiv preprint arXiv:2409.05086*, 2024.
- [21] Y. Li, et al., "Exploration of the configuration and operation rule of the multi-electrolyzers hybrid system of large-scale alkaline water hydrogen production system," *Appl. Energy*, vol. 331, p. 120413, Feb. 2023.
- [22] A. Ibáñez-Rioja, et al., "Off-grid solar PV-wind power-battery-water electrolyzer plant: Simultaneous optimization of component capacities and system control," *Appl. Energy*, vol. 345, p. 121277, Sep. 2023.
- [23] Y. Zheng, S. You, C. Huang, and X. Jin, "Model-based economic analysis of off-grid wind/hydrogen systems," *Renewable Sustain. Energy Rev.*, vol. 187, p. 113763, Nov. 2023.
- [24] ESCN, "Intelli Li Huan: Multiple hydrogen production rectifier solutions, respecting the first principles of technology," 2024. [Online]. Available: <https://www.escn.com.cn/20240827/d9f3804b25104b8ba5101e0e410c6ac0/c.html>
- [25] R. T. Rockafellar and R. J.-B. Wets, "Scenarios and policy aggregation in optimization under uncertainty," *Math. Oper. Res.*, vol. 16, no. 1, pp. 119–147, Feb. 1991.
- [26] The Energy Bureau of Inner Mongolia Autonomous Region, "Implementation guidelines for wind and solar power to ammonia and methanol production projects in Inner Mongolia Autonomous Region," 2024. [Online]. Available: [https://njj.nmg.gov.cn/zwgk/zfxxgkz/fdzdgnr/tzgg\\_16482/gg\\_16484/202409/t20240903\\_2568246.html](https://njj.nmg.gov.cn/zwgk/zfxxgkz/fdzdgnr/tzgg_16482/gg_16484/202409/t20240903_2568246.html)
- [27] Ø. Ulleberg, "Modeling of advanced alkaline electrolyzers: a system simulation approach," *Int. J. Hydrogen Energy*, vol. 28, no. 1, pp. 21–33, Jan. 2003.
- [28] C. Varela, M. Mostafa, and E. Zondervan, "Modeling alkaline water electrolysis for power-to-x applications: A scheduling approach," *Int. J. Hydrogen Energy*, vol. 46, no. 14, pp. 9303–9313, Feb. 2021.
- [29] China Electricity Council, "Technical specification for rectifier power supply in water electrolysis hydrogen production," Standard No. T/CES 226-2023, 2023, in Chinese.
- [30] M. Farivar and S. H. Low, "Branch flow model: Relaxations and convexification—Part I," *IEEE Trans. Power Syst.*, vol. 28, no. 3, pp. 2554–2564, Aug. 2013.
- [31] M. Ghazavi Dozein, O. Gomis-Bellmunt, and P. Mancarella, "Simultaneous provision of dynamic active and reactive power response from utility-scale battery energy storage systems in weak grids," *IEEE Trans. Power Syst.*, vol. 36, no. 6, pp. 5548–5557, Nov. 2021.
- [32] S. Wu, J. Lin, J. Li, F. Liu, Y. Song, Y. Xu, X. Cheng, and Z. Yu, "Multi-timescale trading strategy for renewable power to ammonia virtual power plant in the electricity, hydrogen, and ammonia markets," *IEEE Trans. Energy Mark. Policy Regul.*, vol. 1, no. 4, pp. 322–335, Dec. 2023.
- [33] L. Yang, H. Li, H. Zhang, Q. Wu, and X. Cao, "Stochastic-distributionally robust frequency-constrained optimal planning for an isolated microgrid," *IEEE Trans. Sustain. Energy*, pp. 1–15, 2024.
- [34] Z. Yu, J. Lin, F. Liu, J. Li, Y. Zhao, Y. Song, Y. Song, and X. Zhang, "Optimal sizing and pricing of grid-connected renewable power to ammonia systems considering the limited flexibility of ammonia synthesis," *IEEE Trans. Power Syst.*, vol. 39, no. 2, pp. 3631–3648, Mar. 2024.
- [35] Y. Liu, Y. Chen, H. Xin, J. Tu, L. Zhang, M. Song, and J. Zhu, "System strength constrained grid-forming energy storage planning in renewable power systems," *IEEE Trans. Sustain. Energy*, pp. 1–13, 2024.
- [36] M.-A. Nasr, E. Nasr-Azadani, H. Nafisi, S. H. Hosseini, and P. Siano, "Assessing the effectiveness of weighted information gap decision theory integrated with energy management systems for isolated microgrids," *IEEE Trans. Ind. Inform.*, vol. 16, no. 8, pp. 5286–5299, Aug. 2020.
- [37] J. Li, et al., "Coordinated planning of HVDCs and power-to-hydrogen supply chains for interregional renewable energy utilization," *IEEE Trans. Sustain. Energy*, vol. 13, no. 4, pp. 1913–1929, Oct. 2022.
- [38] T. Liang, M. Chen, J. Tan, Y. Jing, L. Lv, and W. Yang, "Large-scale off-grid wind power hydrogen production multi-tank combination operation law and scheduling strategy taking into account alkaline electrolyzer characteristics," *Renew. Energy*, vol. 232, p. 121122, Oct. 2024.

- [39] Y. Qiu, et al., "Dynamic operation and control of a multi-stack alkaline water electrolysis system with shared gas separators and lye circulation: A model-based study," *arXiv preprint arXiv:2501.14576*, 2025.